

servables are completely independent of this choice. The observables do depend on  $\nu_1$ , however.

<sup>27</sup>L. Wolfenstein, Phys. Rev. **96**, 1654 (1954). See also E. L. Berger and G. C. Fox, Phys. Rev. Letters **25**, 1783 (1970).

<sup>28</sup>A. D. Brody, W. B. Johnson, D. W. G. S. Leith, J. S. Loos, G. J. Luste, K. Moriyasu, B. C. Shen, W. M. Smart, F. C. Winkelmann, R. J. Yamartino, and B. Kehoe, SLAC Report No. SLAC-PUB-823, 1970 (unpublished).

<sup>29</sup>The more nearly EXD behavior at high energies of the  $B$  amplitude than the  $A'$  is popularly understood in terms of Regge-cut contributions [see G. C. Fox, in *High Energy Collisions*, Third International Conference held at State University of New York, Stony Brook, 1969, edited by C. N. Yang, J. A. Cole, M. Good, R. Hwa, and J. Lee-Franzini (Gordon and Breach, New York, 1969), p. 367].

<sup>30</sup>The actual size of the polarization depends not only on the phase difference, but also on the magnitude of the product  $|A'B|$ . From Fig. 10 it can be seen that Eq. (2.12) is approximately satisfied at  $t \approx 0$ .

<sup>31</sup>R. Dolen, D. Horn, and C. Schmid, Phys. Rev. **166**, 1768 (1968).

<sup>32</sup>See also C. Schmid and J. K. Storrow, Nucl. Phys. **B29**, 219 (1971). These authors give arguments to justify the testing of EXD for the  $s$ -channel states at

$t \geq m_{K^*}^2$ . The qualitative features displayed in Fig. 13 also hold at  $t \approx 0$  for  $\text{Im}B$ , and equally for  $\text{Im}A'$ .

<sup>33</sup>M. Ferro-Luzzi, H. K. Shepard, A. Kernan, R. T. Poe, and B. C. Shen, University of California, Riverside, Report No. UCR-P107-114, 1970 (unpublished).

<sup>34</sup>See the Appendix of Ref. 6 for the meaning of these and other technical terms.

<sup>35</sup>D. J. Crennell, Uri Karshon, Kwan Wu Lai, J. S. O'Neill, J. M. Scarr, R. M. Lea, T. G. Schumann, and E. M. Urvater, Phys. Rev. Letters **23**, 1347 (1969).

<sup>36</sup>M. Abramovich, H. Blumenfeld, V. Chaloupka, S. U. Chung, J. Diaz, L. Montanet, J. Pernegr, S. Reucroft, J. Rubio, and B. Sadoulet, Nucl. Phys. **B27**, 477 (1971).

<sup>37</sup>The discrepancies at intermediate energies are currently "explained" by invoking Regge cuts in addition to poles. A. Krzywicki and J. Tran Thanh Van, Phys. Letters **30B**, 185 (1969) are able to fit the behavior of the polarization shown in Fig. 14 by such means.

<sup>38</sup>H. Harari, Ann. Phys. (N.Y.) **63**, 432 (1971), and SLAC Report No. SLAC-PUB-837, 1970 (unpublished).

<sup>39</sup>The shrinkage of the forward peak shown by the SLAC data (Ref. 28) (see Fig. 9) lends circumstantial support to a description of  $K^- n \rightarrow \pi^+ \Lambda$  by Regge poles with little further complication.

<sup>40</sup>For some model calculations, see Chris Quigg, Ph. D. thesis, LRL Report No. UCRL-20032, 1970 (unpublished).

## Rotation of the Symmetry Axis in $K\pi$ Scattering\*

W. E. Slater

Department of Physics, University of California at Los Angeles, Los Angeles, California 90024

(Received 12 April 1971)

The failure of the Treiman-Yang test of one-pion exchange in the reactions  $K^+p \rightarrow K^0\pi^0\Delta^{++}$  and  $K^+\pi^-\Delta^{++}$  for c.m. energies from 2.5 to 5.0 GeV is shown to have a simple dependence on  $t'$ . We find an empirical dynamic  $z$  axis with respect to which the  $K$ -meson angular distributions are independent of azimuth. This axis, which depends on  $t'$ , is seen to be equivalent to the axis of Donohue and Högaasen in the neighborhood of the  $K^*(0.89)$ .

In a calculation based on the absorption model of Gottfried and Jackson,<sup>1</sup> Donohue and Högaasen<sup>2</sup> suggested the use of a "dynamic" reference frame in which the density matrix describing the decay of a vector meson (e.g.,  $\rho$  or  $K^*$ ) is diagonal. This frame differs from the usual  $t$ -channel (Jackson) frame<sup>3</sup> by a rotation. Experimentally, such effects have been noted in several final states<sup>4</sup> of reactions induced by  $\pi^+$  mesons and photons on hydrogen. We first noted the rotation in a sample of 4850 events of reaction (1a) and 703 events of reaction (1b) at 7.3 GeV/c,

$$K^+p \rightarrow K^+\pi^-\Delta^{++}, \quad (1a)$$

$$K^+p \rightarrow K^0\pi^0\Delta^{++}. \quad (1b)$$

To confirm the existence of the effect and to look

at the  $s$ ,  $t$ , and  $M_{K\pi}$  dependences, we have used the world  $K^+p$  collaboration data<sup>5</sup> consisting of 37 152 events of reaction (1a) and 6592 events of reaction (1b). We note that analogous effects, *prima facie*, have been understood in the angular distribution of photons produced by inelastic scattering of protons on nuclei<sup>6</sup>; a simple model leading to the same effect in inelastic  $\alpha$ -nucleus scattering was described by Inglis<sup>7</sup> and this rotation was observed in many experiments.<sup>8</sup>

If one assumes that a single-pion-exchange mechanism dominates the low-momentum-transfer [ $t = (P_{\text{target}} - P_{\Delta})^2$ ] region of reactions (1), as in Fig. 1(a), then an appropriate coordinate system in which to study the final-state  $K$ -meson angular distribution was defined by Jackson<sup>3</sup> such that the

$K^+\pi^0$  system is at rest, the  $z$  axis is along the incident  $K^+$  (viewed in this rest frame), and the  $y$  axis is the production plane normal [defined here as  $(\vec{p} \times \vec{\Delta})/|\vec{p} \times \vec{\Delta}|$ ]. Most  $K\pi$  scattering studies have considered angular-distribution moments of  $K_{\text{out}}$  as functions of  $M_{K\pi}$  and  $t$ , and have attempted to extrapolate them in  $t$  to the pion pole<sup>9</sup> to describe on-mass-shell  $K\pi$  scattering, or have extrapolated partial cross sections.<sup>10</sup>

A persistent and troublesome aspect of this topic has been the presence of significantly nonzero moments with  $m \neq 0$ . These appear to vanish as  $|t|$  minimum, as they must since the production plane loses definition there. These moments describe azimuthal asymmetry which can be seen in the Treiman-Yang angle plots of Figs. 1(b) and 1(d). The only cut made in the data was to select  $\Delta^{++}$ ,  $1.13 \leq M_{\pi^+\rho} \leq 1.33 \text{ GeV}/c^2$ . Unadorned pion exchange would predict both distributions to be flat.<sup>11</sup>

To demonstrate the origin of the anisotropy of Fig. 1(d) we made a further cut on the data to select  $K^*(0.89)$  ( $0.84 \leq M_{K\pi} \leq 0.94 \text{ GeV}/c^2$ ) in reaction (1a), and for three choices of momentum-transfer cutoff we plot the  $\cos\theta$  distributions in Fig. 2(a).

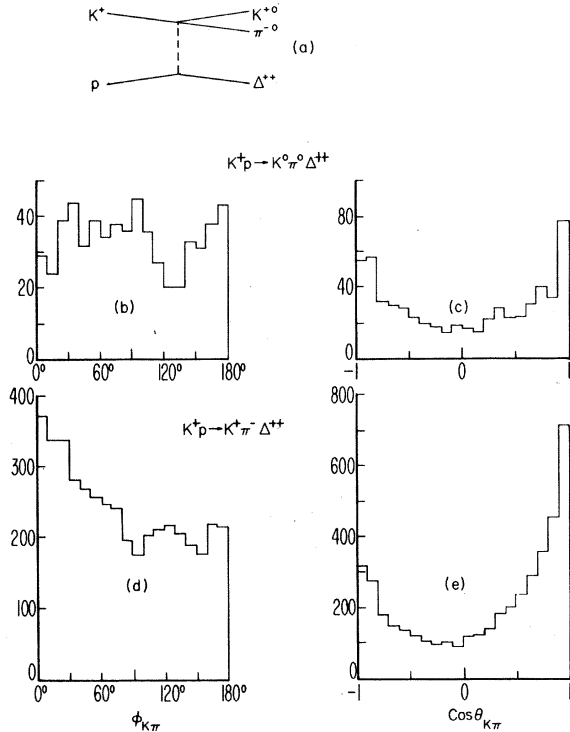


FIG. 1. (a) Diagram for elastic and charge-exchange virtual  $\pi$ - $K$  scattering. (b) Treiman-Yang angle (folded with respect to the production plane) at the  $K\pi$  vertex for  $K^+p \rightarrow K^0\pi^0\Delta^{++}$  at  $7.3 \text{ GeV}/c$ . (c) Jackson angle at the  $K\pi$  vertex for  $K^+p \rightarrow K^0\pi^0\Delta^{++}$  at  $7.3 \text{ GeV}/c$ . (d) Same as (b) but for  $K^+p\pi^-\Delta^{++}$  final state. (e) Same as (c) but for  $K^+p\pi^-\Delta^{++}$  final state.

The corresponding Treiman-Yang distributions are shown in Fig. 2(b) and one notes that the anisotropy diminishes at small  $t' = t - t_{\text{min}}$ . Figures 2(c) and 2(d) show the Treiman-Yang distributions separately for the backward ( $\cos\theta < 0$ ) and forward emitted  $K$ 's, respectively. Significantly, these peak at  $\phi = 0^\circ$  and  $180^\circ$ , respectively, when the  $t'$  cut is large. A similar effect would obtain if one described the distribution in longitude of ice at the earth's north and south poles but used a  $z$  axis intersecting the Arctic circle instead of the axis of rotation.

To show that this shift of symmetry axis is the origin of the anisotropy in Figs. 1(d) and 2(b), we tried to define a suitable  $z'$  axis to study the  $K\pi$  angular distributions. The work of Donohue and Högaasen is strictly applicable only to the  $p$ -wave part of the  $K\pi$  scattering amplitude, since it is based on diagonalizing the real part of a  $3 \times 3$  spin-density matrix. Nevertheless, we have, as a first approximation, calculated the angle  $\theta$  by which the dynamic  $z'$  axis is rotated about the production plane normal with respect to the Jackson  $z$  axis in the  $K\pi$  rest frame using the formula (2d) of Donohue and Högaasen:

$$\tan(2\theta) = \frac{-2\sqrt{2} \text{Re}\rho_{10}}{\rho_{00} - \rho_{11} + \rho_{1,-1}} \quad (2)$$

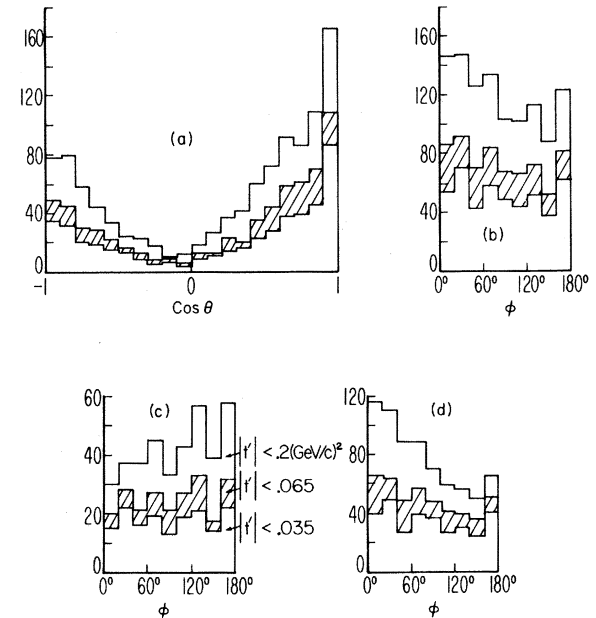


FIG. 2. (a) Jackson angle for  $K^+p \rightarrow K^0\pi^0\Delta^{++}$  at  $7.3 \text{ GeV}/c$  with cuts on momentum transfer of  $|t'| < 0.2, 0.065, 0.035 \text{ (GeV}/c)^2$ . (b) Treiman-Yang angle (folded) for the same cuts as in (a). (c) Treiman-Yang angle (folded) for the events of (a) with  $\cos\theta < 0$ . (d) Same as (c) but for  $\cos\theta > 0$ .

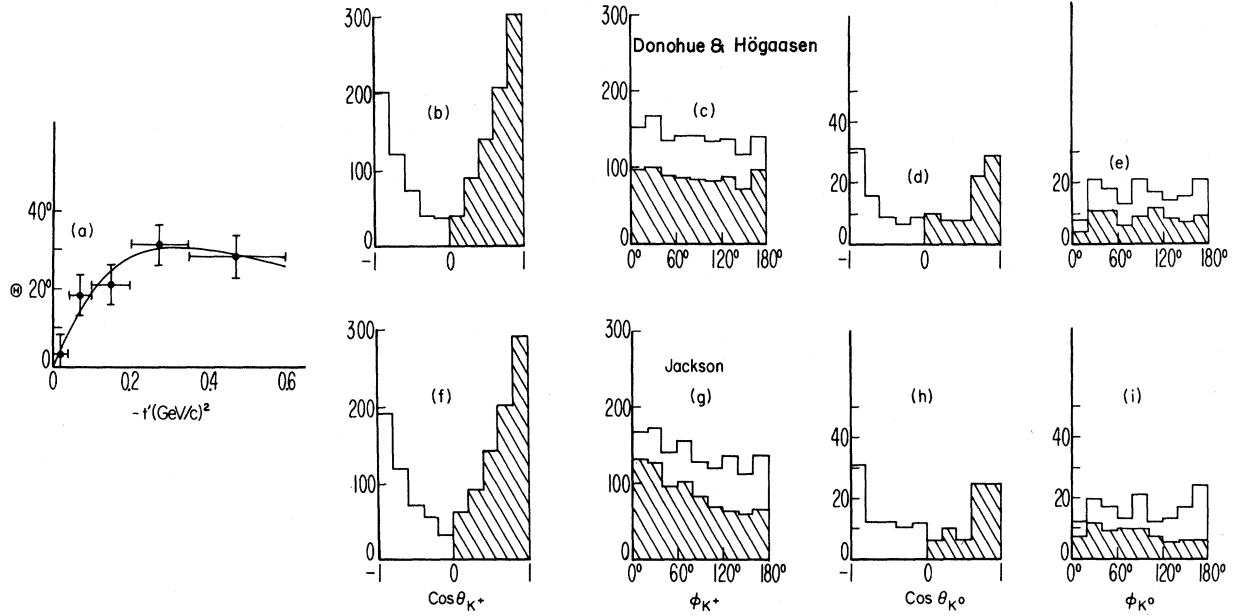


FIG. 3. (a) Donohue-Högaasen angle for  $K^+p \rightarrow K^*(0.89)\Delta^{++}$ ,  $K^* \rightarrow K^+\pi^-$  at 7.3 GeV/c as a function of momentum transfer above kinematic cutoff. Mass cuts:  $0.84 < M_{K\pi} < 0.94 \text{ GeV}/c^2$ ;  $1.13 < M_{\pi^+p} < 1.33 \text{ GeV}/c^2$ . (b), (c) Colatitude and azimuth for events of (a) using the "dynamic  $z'$  axis" (see Ref. 2). The azimuth is folded with respect to the production plane. (d), (e) Same as (b) and (c) but for the  $K^0\pi^0$  final state. (f), (g), (h), (i) Same as (b), (c), (d), (e) but using the Jackson axes.

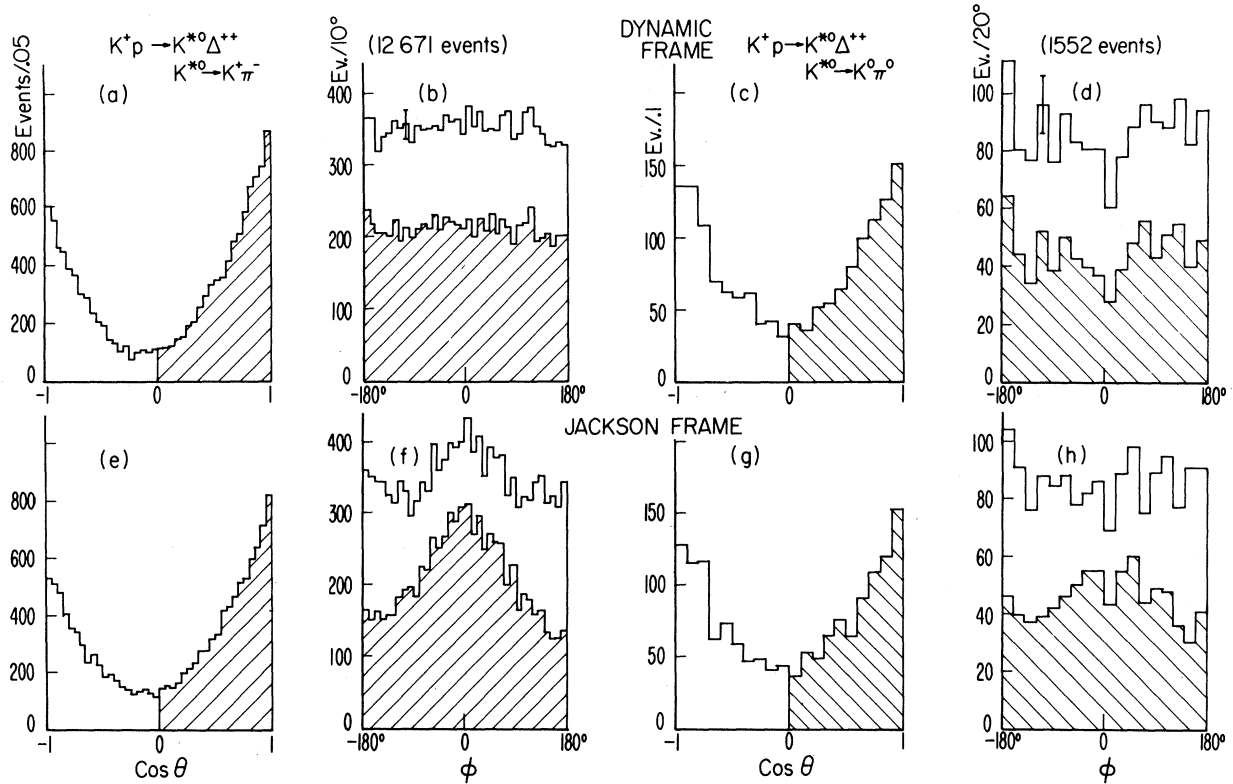


FIG. 4. (a)-(d) Colatitude and azimuth for the world  $K^+p \rightarrow K^{*0}\Delta^{++}$  data in the dynamic frame determined from Eq. (3) of the text. (e)-(h) Same for the Jackson frame. The  $K^+\pi^-$  data alone were used to determine the dynamic  $z'$  axis. Mass cuts:  $0.84 < M_{K\pi} < 0.94 \text{ GeV}/c^2$ ,  $1.13 < M_{\pi^+p} < 1.33 \text{ GeV}/c^2$ .

To determine the dynamic  $z'$  axis in this way is essentially an *ad hoc* procedure and does not reveal much about the physical reason for the rotation, which if one believes the nuclear-physics analogy, is connected with the fact that our incident particles,  $\pi^-$  at the  $K\pi$  vertex or  $\pi^+$  at the  $p\pi^+$  vertex, are not free-particle states, but should be described by a distorted plane wave. The results for  $\theta$  as a function of  $t'$  are shown in Fig. 3(a). The hand-drawn curve in that plot is a smooth approximation to the data.

When we use a  $z'$  axis, determined for each event as a function of  $t'$  alone based on the curve of Fig. 3(a), we obtain the  $\cos\theta'$  and  $\phi'$  distributions of Figs. 3(b) and 3(c). These are shown for all the events and also for the subsample with  $\cos\theta' > 0$ . The pile-up at  $\phi' \approx 0$  is considerably diminished for the "elastic" events [reaction (1a)]. Similar results [Figs. 3(d) and 3(e)] hold for the charge-exchange events [reaction (1b)]. Figures 3(f), 3(g), 3(h), and 3(i) show these distributions using the Jackson  $z$  axis. Qualitatively, the net Treiman-Yang distribution for the charge-exchange reaction is nearly flat because the peak

at  $\phi = 0$  for forward emitted  $K^0$ 's nearly fills in the depletion at  $\phi = 0$  for the backward  $K^0$ 's. This can happen since the forward and backward peaks are almost equally populated [see Figs. 3(d) and 3(h)]. For the elastic events, the front-back asymmetry is large ( $\sim 2:1$ ) so that the forward and backward poles do not compensate each other [Figs. 3(b) and 3(f)]. We show identical and more convincing distributions for the world data in Figs. 4(a)–4(h); the  $z'$  axis was determined by a procedure described below.

Next, we see what happens to the  $K\pi$  moments for the 7.3-GeV/ $c$  data. Figure 5 shows the  $\langle Y_l^m \rangle$  moments for  $1 \leq l \leq 4$ ;  $m \leq 1$  for the Jackson axes. All the  $\langle Y_l^1 \rangle$  moments are nonzero over substantial  $M_{K\pi}$  ranges, for this choice of momentum-transfer cut,  $|t'| < 0.5$  (GeV/ $c$ )<sup>2</sup>. The same moments, using the dynamic  $z'$  axis are plotted in Fig. 6. The  $\langle Y_l^1 \rangle$  moments here are consistent with zero except near  $M_{K\pi} = 1.4$  GeV/ $c$ <sup>2</sup>. The  $\langle Y_l^0 \rangle$  moments are qualitatively the same as Fig. 5, although the magnitudes are somewhat larger, especially for  $l=3,4$ . Since these moments involve higher powers of  $\cos\theta$  they are more sensitive to a misalignment of the  $z$  axis. It is significant that this rotation reduces the magnitude of every  $\langle Y_l^1 \rangle$  moment and increases all the  $\langle Y_l^0 \rangle$  moments

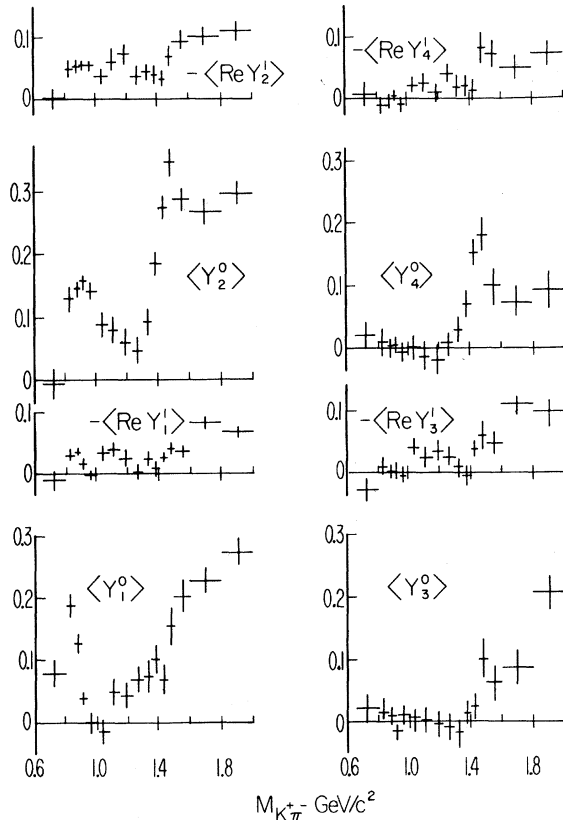


FIG. 5.  $K^+\pi^-$  angular-distribution moments for  $K^+p \rightarrow K^+\pi^-\Delta^{++}$  at 7.3 GeV/ $c$  in the Jackson frame. Cuts on the data:  $1.13 < M_{\pi^+p} < 1.33$  GeV/ $c$ <sup>2</sup>;  $|t'| < 0.5$  (GeV/ $c$ )<sup>2</sup>.

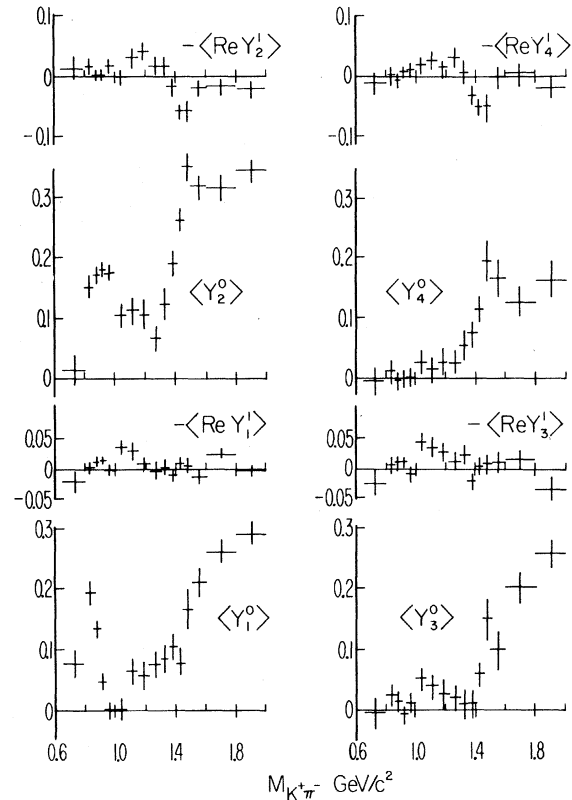


FIG. 6. Same as Fig. 5 but using the dynamic  $z'$  axis.

throughout the range of  $M_{K\pi}$ .

To describe the rotation in a wider region of  $M_{K\pi}$  than just the  $p$ -wave  $K^*(0.89)$ , we use the well-known transversity frame, taking a polar axis  $\hat{\zeta}$  as normal to the production plane,  $\hat{\xi}$  as the incident  $K^+$  direction, and  $\hat{\eta} = \hat{\zeta} \times \hat{\xi}$ .  $\theta_s$  is the colatitude of the outgoing  $K$  meson in the neutral  $K\pi$  frame measured from the  $\zeta$  axis and  $\phi_s$  is its azimuth in the  $\xi$ - $\eta$  plane. In Fig. 7(a) we show the  $\phi_s$  projection of our  $K^*(0.89) - \Delta^{++}$  events at 7.3 GeV/c. The strongly polar Jackson-angle distribution shows up here as a double-peaked structure, and the fore-aft asymmetry is manifest in the unequal heights of the  $\phi_s$  peaks. What is shown clearly in Fig. 7(a) is the Donohue-Högaasen rotation: The  $\phi_s$  peaks are displaced from the  $\pm \xi$  axes by approximately  $+20^\circ$ . To be certain that the rotation is about our  $\zeta$  axis, we show the  $\cos\theta_s$  distributions for "forward"  $K^+$ s ( $-70^\circ < \phi_s < 110^\circ$ ) in Fig. 7(b) and for "backward" ones in Fig. 7(c). No displacement of the poles of the distributions from  $\theta_s = 90^\circ$  is detectable. Returning to consider  $\phi_s$ , Fig. 7(a) suggests an empirical way to measure the rotation  $\phi_0$  needed to make the distributions show peaks at  $\phi'_s \equiv \phi_s - \phi_0$  values of  $0^\circ$  and  $180^\circ$ . Namely, we minimize

$$\chi^2(\phi_0) = \sum_{\text{bins}} \frac{[N_i(\phi_s) - N_i(-\phi_s')]^2}{N_i(\phi_s') + N_i(-\phi_s')} \quad (3)$$

We first worked with the  $K^*(0.89)$  band since the results may be compared to those from equation (2) and statistical uncertainties are small. We used events from the world  $K^+$  collaboration data tape of 1970 including our 7.3-GeV/c data (37200  $K^+\pi^-\Delta^{++}$  events). From the UCLA data alone [Fig. 3(a)] it is clear that  $\phi_0$  rises rapidly with increasing  $t'$  near  $t'=0$ . Therefore, we selected  $0.05 < |t'| < 1.00$  (GeV/c)<sup>2</sup>, and determined  $\phi_0$  as a function of  $\sqrt{s}$ . We used  $10^\circ$  bins in  $\phi_s$  so that  $\chi^2(\phi_0)$  is based on 18 degrees of freedom. The errors quoted in the following measurements are for a 10% confidence level ( $\chi^2=26$ ). In each case, the best-fit  $\chi^2$  was less than 20, corresponding to a confidence level of 35%. In Fig. 8(a), where we show  $\phi_0$  vs  $\sqrt{s}$ , there is evidently no detectable dependence on  $\sqrt{s}$  between 2.5 and 5.0 GeV. We therefore combined all these experiments to look more closely at the  $t'$  dependence, shown in Fig. 8(b) for the  $K^*(0.89)$  band. A straight line would evidently fit these data very well; its equation is

$$\phi_0[\ln(t'/t'_0)] = (19^\circ \pm 2^\circ) + (7.4^\circ \pm 1.7^\circ) \ln(t'/t'_0),$$

where  $t'_0 = 0.1$  (GeV/c)<sup>2</sup>. In Fig. 8(c) we plot  $\chi^2(\phi_0)$  for the points shown in Fig. 8(b). All of these correspond to confidence levels greater than 70%. The  $\phi_s$  distribution is given in Fig. 8(d) for  $0.04 < |t'| < 1.00$  (GeV/c)<sup>2</sup>. A value of  $\phi_0$  for  $s$  near threshold was determined in a preliminary sample

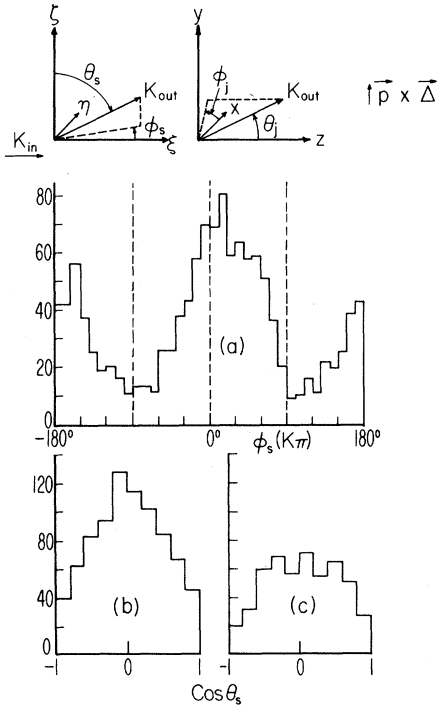


FIG. 7. (a) Azimuth distribution for  $K^+\pi^- \rightarrow K^*(0.89)\Delta^{++}$ ,  $K^*\pi^- \rightarrow K^+\pi^-$  at 7.3 GeV/c.  $\zeta$  axis = production-plane normal ( $\hat{\zeta} \sim \vec{p}_{\text{target}} \times \vec{\Delta}$  in the  $K^*$  rest frame), the  $\xi$  axis is the direction of the incident  $K^+$  in this frame. Cuts on data:  $|t'| < 1$  (GeV/c)<sup>2</sup>;  $0.84 < M_{K\pi} < 0.94$  GeV/c<sup>2</sup>;  $1.13 < M_{\pi^+\pi^-} < 1.33$  GeV/c<sup>2</sup>. (b) Colatitude distribution for  $-70^\circ < \phi_s < 110^\circ$ . (c) Same as (b) but for  $110^\circ < \phi_s < 290^\circ$ .

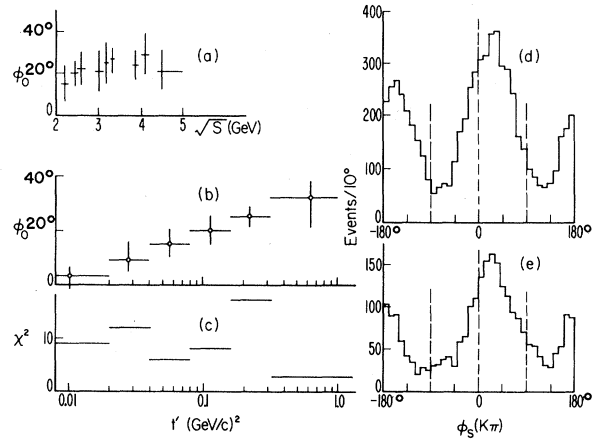


FIG. 8. (a)  $K\pi$  symmetry-axis rotation ( $\phi_0$ ) with respect to the incident  $K^+$  as a function of  $\sqrt{s}$ . Data are from Refs. 5 and 12 in addition to our point at  $\sqrt{s} = 3.9$  GeV. Cuts:  $1.13 < M_{\pi^+\pi^-} < 1.33$  GeV/c<sup>2</sup>;  $0.84 < M_{K\pi} < 0.94$  GeV/c<sup>2</sup>;  $0.05 < |t'| < 1$  (GeV/c)<sup>2</sup>. (b)  $\phi_0$  as a function of  $t'$  using the data in (a) for which  $\sqrt{s} > 2.5$  GeV. (c) Minimum  $\chi^2$  [see text, Eq. (3)] for the  $\phi_0$  values of (b). (d) Distribution of  $\phi_s$  (see text) for events used in (b) with the additional cut  $0.05 < |t'| < 1$  (GeV/c)<sup>2</sup>. (e) Same as (d) but for the  $d$ -wave  $K^*(1.4)$ .  $1.3 < M_{K^+\pi^-} < 1.5$  GeV/c<sup>2</sup>.

of reaction (1a) for  $\sqrt{s} \approx 2.2$  GeV.<sup>12</sup> This point is shown on Fig. 8(a) and it suggests that  $\phi_0$  may diminish at threshold.

Equivalence of this rotation by  $\phi_0$  with the Donohue-Högaasen rotation is seen empirically: (1) Both rotations are about the production plane normal. (2) The  $m \neq 0$  moments now vanish [ $\langle \text{Re} Y_2^2 \rangle = 0.0 \pm 0.002$ ,  $\langle \text{Re} Y_1^1 \rangle = 0.001 \pm 0.002$ ,  $\langle \text{Re} Y_1^0 \rangle = -0.003 \pm 0.002$  for  $0.84 < M_{K\pi} < 0.94$  GeV/c<sup>2</sup> and  $|t'| < 0.1$  (GeV/c)<sup>2</sup>. For the same cuts  $\langle Y_2^0 \rangle = 0.190 \pm 0.003$  and  $\langle Y_1^0 \rangle = 0.081 \pm 0.004$ .] (3) Consequently, the  $\phi$  distributions [Figs. 4(b) and 4(d)] are flat. (4) The density-matrix elements calculated from  $\langle Y_2^0 \rangle$ ,

$\langle \text{Re} Y_2^1 \rangle$ , and  $\langle \text{Re} Y_2^2 \rangle$  are  $\text{Re} \rho_{10} = -0.003 \pm 0.006$ ,  $\rho_{1-1} = 0.0 \pm 0.006$ , and  $\rho_{00} = 0.838 \pm 0.005$ , so that  $\text{Re} \rho$  is diagonal.

The situation for other  $M_{K\pi}$  intervals is less clear. Qualitatively, it is apparent that a symmetry-axis rotation occurs in Fig. 8(e) which shows  $\phi_s$  for the  $d$ -wave  $K^*(1.4)$  region, ( $1.3 < M_{K\pi} < 1.5$  GeV/c<sup>2</sup>). The forward and backward peaks are displaced from 0° and 180°, respectively, by 10°–20°. The distribution is not, however, as symmetric as Fig. 8(d) for the  $K^*(0.89)$ . There is an excess of events in Fig. 8(e) in the region  $30^\circ < \phi_s < 120^\circ$ , the effect of which on our determinations of

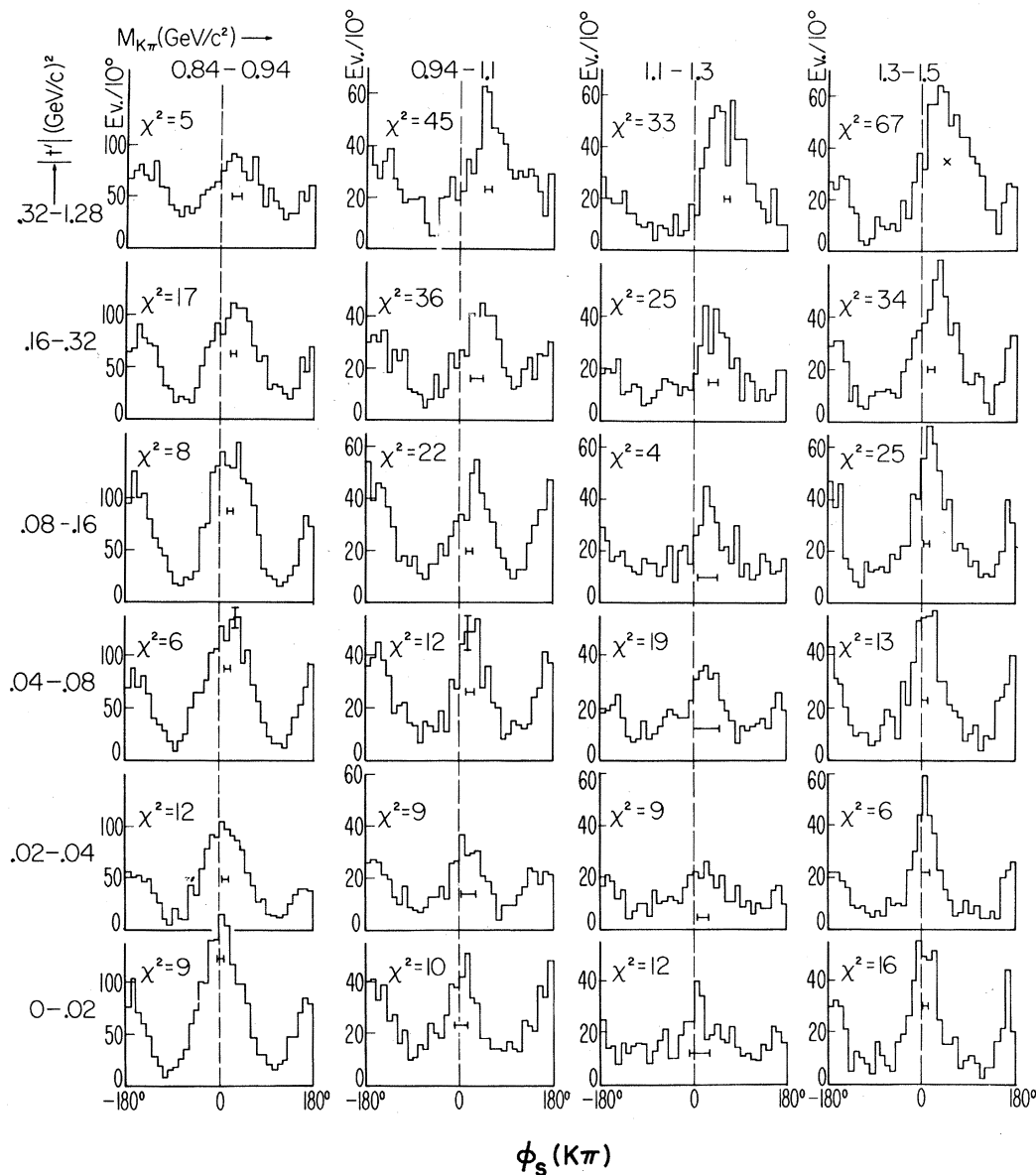


FIG. 9. Azimuth distributions in the  $K^+ \pi^-$  transversity frame for  $K^+ p \rightarrow K^+ \pi^- \Delta^{++}$ , shown as functions of  $M_{\pi K}$  and  $t'$ . Cuts on data:  $1.13 < M_{\pi K} < 1.33$  GeV/c<sup>2</sup>. The bar symbols show  $\phi_0$  for each plot.

TABLE I. Rotation of the symmetry axis for the  $K^+\pi^-$  system as a function of  $M_K$  and  $t'$ . For  $\chi^2(\phi_0) > 20$ , the error in  $\phi_0$  corresponds to  $\chi^2 = \chi^2(\phi_0) + 10$ . For  $\chi^2 < 20$ , the error in  $\phi_0$  corresponds to  $\chi^2 = 26$  (10% confidence level).

$-t'$ (GeV/c) <sup>2</sup>	$M_K$ (GeV/c <sup>2</sup> )		0.84–0.94		0.94–1.1		1.1–1.3		1.3–1.5	
	$\phi_0$ (deg)	$\chi^2$	$\phi_0$ (deg)	$\chi^2$	$\phi_0$ (deg)	$\chi^2$	$\phi_0$ (deg)	$\chi^2$	$\phi_0$ (deg)	$\chi^2$
0–0.02	$3_{-3}^{+3}$	9	$2 \pm 13$	10	$11 \pm 20$	12	$7 \pm 5$	16		
0.02–0.04	$9_{-4}^{+7}$	12	$13 \pm 15$	9	$17 \pm 20$	9	$9_{-4}^{+5}$	6		
0.04–0.08	$15 \pm 5$	6	$21 \pm 8$	12	$23 \pm 25$	19	$7 \pm 5$	13		
0.08–0.16	$20 \pm 5$	8	$19 \pm 5$	22	$28 \pm 20$	4	$11 \pm 5$	25		
0.16–0.32	$25 \pm 4$	17	$32 \pm 11$	36	$38 \pm 10$	25	$18 \pm 6$	34		
0.32–1.28	$32_{-11}^{+5}$	5	$52_{-4}^{+7}$	45	$62 \pm 5$	33	45	67		

$\phi_0$  is to yield large values for  $\chi^2(\phi_0)$ ; the excess is more severe as  $t'$  increases. This “right-left” asymmetry is difficult to reconcile with any simple model of  $\pi$ - $K$  scattering, and is more likely the result of  $\pi^- \Delta^{++}$  final-state interactions. In fact, there are peaks in the  $M_{\pi^- \Delta^{++}}$  distribution of events in the forward region  $-60^\circ < \phi_s < 120^\circ$  (not shown) near  $M_{\pi \Delta} \simeq 1.5$  GeV/c<sup>2</sup> and  $M_{\pi \Delta} \simeq 1.68$  GeV/c<sup>2</sup>, where  $N^*$ 's are known to have substantial  $N\pi\pi$  and  $\pi\Delta$  decay rates. These  $N^*$ 's are much less significant in the  $M_{\pi \Delta}$  distribution for the  $K^*(0.89)$  events, even though the kinematically available  $M_{\pi \Delta}$  region is nearly the same.

Figure 9 presents a qualitative picture of the  $M_{K\pi}$  and  $t'$  dependences of these  $\phi_s$  distributions. Table I summarizes the results for  $\phi_0$  and  $\chi^2(\phi_0)$ . We see that the distributions retain “right-left” symmetry as  $|t'|$  increases, in the region of the  $K^*(0.89)$ , if the “forward” direction is taken as  $\phi_s = \phi_0$ . In the other  $M_{K\pi}$  regions, the  $\phi_s$  distributions all lose right-left symmetry for  $|t'| > 0.1$  (GeV/c)<sup>2</sup> even with respect to a shifted axis. We suggest that the  $p$ -wave  $K^*(0.89)$  is sufficiently long lived that it dominates the  $K\pi$  angular distributions while the region much above  $M_{K\pi} = 0.94$  GeV/c<sup>2</sup> is seriously distorted by overlapping  $N^* \rightarrow \pi^- \Delta^{++}$  decays which naturally produce the observed right-left asymmetries as  $|t'|$  increases. Unless this kind of background can be reliably subtracted and until the symmetry-axis rotation is taken into account, there is little hope of extracting  $K\pi$  scattering amplitudes from the angular distributions. The problem of overlapping  $\pi^- \Delta^{++}$  final-state interactions does not necessarily vanish as  $t' \rightarrow 0$ ; experimentally, the right-left asymmetry which could partially resolve that interaction from the  $K\pi$  interaction, goes to zero because at  $t' = 0$  the  $\pi^- \Delta^{++}$  effective mass depends only on the Jackson angle  $\theta$  and not on the Treiman-Yang angle  $\phi$ .

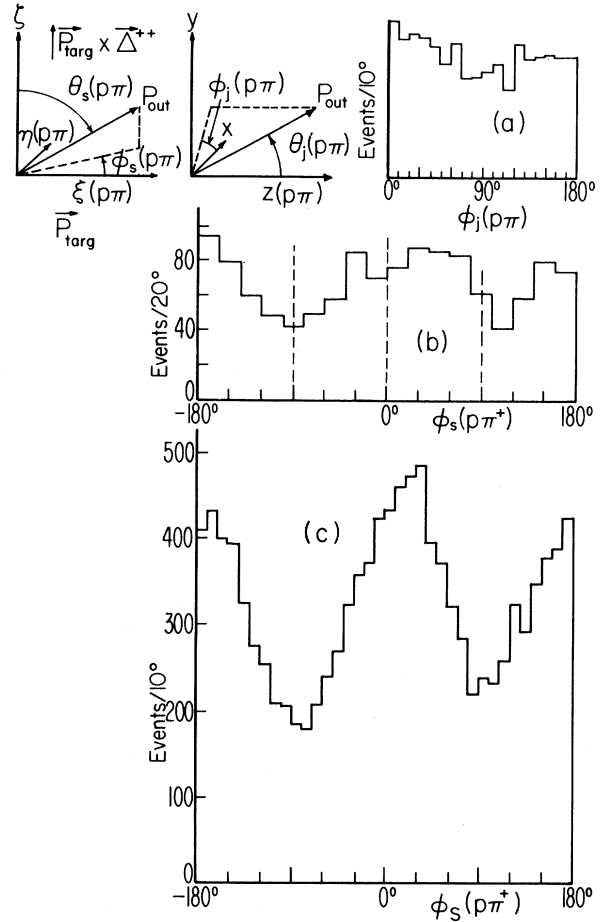


FIG. 10. (a) Treiman-Yang distribution at the  $\pi^+p$  vertex. Cuts on data:  $\sqrt{s} \simeq 3.9$  (present experiment),  $0.84 < M_{K^+\pi^-} < 0.94$  GeV/c<sup>2</sup>;  $1.13 < M_{\pi^+p} < 1.33$  GeV/c;  $|t'| < 0.5$  (GeV/c)<sup>2</sup>. (b) Distribution of  $\phi_s(p\pi^+)$  (see text for definition).  $\phi_s(p\pi^+) = 0$  for outgoing protons parallel to the incoming target proton [ $\xi(p\pi^+)$  axis]. Same events as in (a). (c) Same distribution as (b) but using  $K^+$  collaboration data with  $\sqrt{s} > 2.5$  GeV (Ref. 5).

It is of interest to examine whether a rotation of the symmetry axis is present in the  $\pi^+p$  system. The  $\pi^+p$  azimuth,

rest frame:  $\pi^+p$ ,

$z$  axis =  $\hat{p}_{\text{target}}$ ,

$y$  axis =  $\vec{K}_{\text{inc}} \times \vec{K}^+ \pi^- / |\vec{K}_{\text{inc}} \times \vec{K}^+ \pi^-|$ ,

shows a slight pile-up at  $\phi = 0^\circ$ , as seen in Fig. 10(a), similar to the  $K^+ \pi^-$  Treiman-Yang distribution. We selected here our  $K^*(0.89)\Delta^{++}$  events

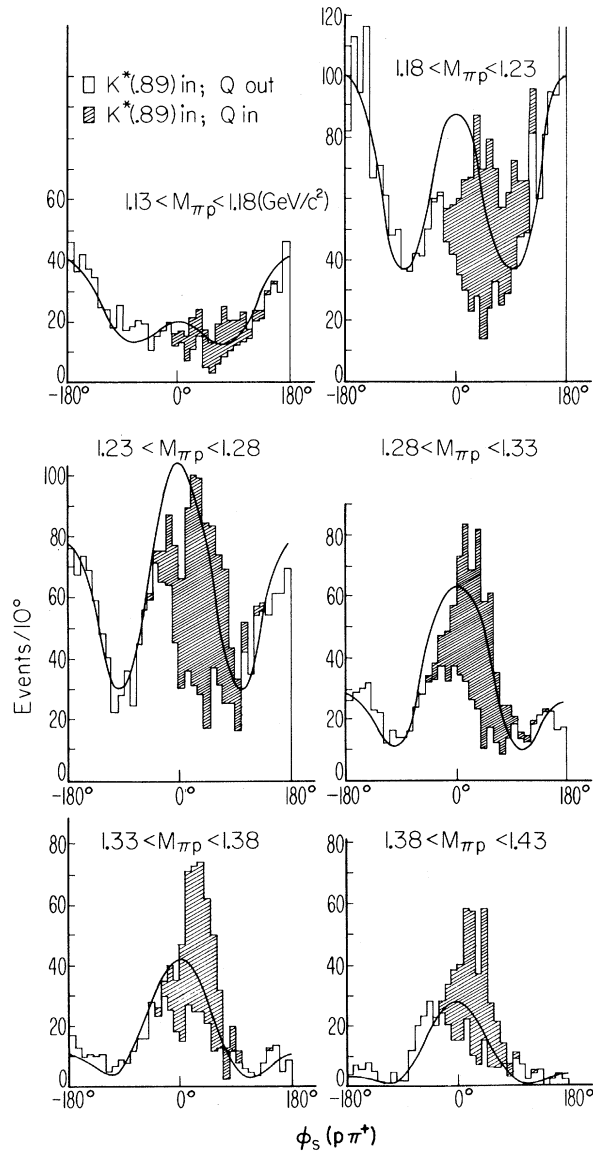


FIG. 11. (a)–(f) Azimuth distributions in the  $p\pi^+$  trans-versity frame for  $K^+p \rightarrow K^{*0}\Delta^{++}$ ,  $K^* \rightarrow K^+\pi^-$ . Events where the  $\pi^+K^*$  are in the  $Q$  region  $1.1 < M_{K^*\pi^-} < 1.4$   $\text{GeV}/c^2$  are shaded. Cuts on data:  $P_{\text{lab}} > 4$   $\text{GeV}/c$ ,  $0.84 < M_{K^+\pi^-} < 0.94$   $\text{GeV}/c^2$ ,  $0.02 < |t'| < 2.0$   $(\text{GeV}/c)^2$ .

with  $|t'| < 0.5$   $(\text{GeV}/c)^2$ . As at the  $K\pi$  vertex we use the production-plane normal as  $\xi$  axis; the  $\xi(p\pi)$  axis is taken as the direction of the target proton viewed in the  $p\pi^+$  frame. In Fig. 10(b) we show the  $\phi_s(p\pi^+)$  distribution for these events. The peaks in this distribution are not so prominent as for  $\phi_s(K\pi)$ , Fig. 8(d); however, a similar rotation of the symmetry axis appears to be present here and in the combined  $K^+$  collaboration data as shown in Fig. 10(c).

One aspect of these plots leads us to look for non- $\Delta^{++}$  effects, however: namely, the fact that the valley at  $\phi_s(p\pi^+) \cong -90^\circ$  is deeper than the one at  $\phi_s(p\pi^+) \cong +90^\circ$ . This corresponds to a “right-left” asymmetry similar to the one in Fig. 8(e) but more pronounced. The cause of the asymmetry becomes clear when we plot  $\phi_s(p\pi^+)$  for small  $M_{\pi p}$  ranges and distinguish events where the  $\pi^+$  and the  $K^*$  are in the  $Q$  region,  $1.1 < M_{K^+\pi^-} < 1.4$   $\text{GeV}/c^2$ . Figures 11(a)–11(f) show these plots; the  $Q$  events populate mainly the quadrant from  $-20^\circ < \phi_s(p\pi^+) < 70^\circ$  and clearly distort what might otherwise be interpreted as off-shell  $\pi^+p$  scattering. Judging from the  $M_{K\pi\pi}$  spectrum (not shown), the actual  $Q$  signal above background is about  $\frac{1}{3}$  of the events shaded in Figs. 11(a)–11(d).

For comparison, and to estimate the size of this distortion, we calculated  $\phi_s$  for on-mass-shell  $\pi^+p$  scattering,<sup>13</sup> and normalized the calculation to the backward peak [ $\phi_s(p\pi^+) \cong 180^\circ$ ] of the lowest ( $1.13 < M_{\pi p} < 1.18$   $\text{GeV}/c^2$ ) region in which the  $Q$  overlap is least significant. The resulting curves are shown on Figs. 11(a)–11(f). If we look only at the backward peaks, there are more events in the regions  $-180^\circ < \phi_s(p\pi^+) < -130^\circ$  than in the ones  $130^\circ < \phi_s(p\pi^+) < 180^\circ$ , and these consistent though small deviations throughout the  $\Delta$  region suggest there is a symmetry-axis rotation. The forward peaks are sufficiently distorted by the overlapping  $Q$  events, however, that we cannot measure the rotation. From Figs. 11(e)–11(f) it appears evident that since the decay angular distribution contains only a forward peak in this  $M_{\pi p}$  range, there is no way to differentiate between a Donohue-Högaasen rotation at the  $\pi^+p$  vertex and a low-mass final-state interaction  $Q \rightarrow K^{*0}\pi^+$ . As noted above, this problem becomes more severe at small  $t'$ . At zero  $t'$ , the  $t$ -channel, helicity, and Donohue-Högaasen  $z$  axes all coincide; thus the data peak for  $\phi_s(p\pi^+) = 0^\circ$  and  $180^\circ$ , and the  $Q$  populates the peak at  $\phi_s = 0^\circ$ . These particular overlapping effects would be resolved at higher beam momenta.

## CONCLUSIONS

We have found a striking regularity in the angular distributions of reactions frequently interpret-



ed in terms of  $K\pi$  scattering in a single-pion-exchange model: The outgoing  $K^+$ 's, in the  $K\pi$  rest frame, are distributed symmetrically not about the "incident-particle" direction but about a direction rotated on the average approximately  $20^\circ$  in the production plane with respect to the incident  $K^+$ . For the  $p$ -wave  $K^*(0.89)$ , the amount of rotation is nearly independent of  $s$ ; it is zero for minimum momentum transfer and roughly logarithmic in  $t'$  for  $|t'| > 0.02$  (GeV/c)<sup>2</sup>. A rotation is present for other  $K\pi$  effective-mass regions, but knowledge of a detailed dependence on  $M_{K\pi}$  has not been possible, owing to the presence of overlapping  $N^* \rightarrow \pi^-\Delta^{++}$  decays.

The effect of this rotation is probably less important in cross-section extrapolations than in extrapolations of angular-distribution moments. Since

the symmetry axis shifts rapidly in the region  $|t'| < 0.04$  (GeV/c)<sup>2</sup>, it is not clear that an *ad hoc* extrapolation of angular-distribution moments is adequate to go from physical values of  $t$  to  $t = +M_\pi^2 c^2$ . A more fundamental problem is to distinguish  $K\pi$  scattering from a  $\pi^-\Delta^{++}$  final-state interaction, or at the lower vertex,  $\pi^+p$  scattering from the  $Q$ . We have seen that a relatively small  $Q$  signal appreciably distorts the  $\pi^+p$  angular distribution. The lack of right-left symmetry in the  $\phi_s(K\pi)$  distributions outside the  $K^*(0.89)$  region indicates that final-state  $N^* \rightarrow \pi^-\Delta^{++}$  decays produce a non-negligible effect on these distributions. Within the  $K^*(0.89)$  region, the  $\phi_s$  distribution has right-left symmetry for essentially all values of  $t'$  once one chooses what is equivalent to the Donohue-Högaasen coordinate system.

\*Supported by the U. S. Atomic Energy Commission under Contract No. AEC AT (11-1) Gen. 10, Project 17.

<sup>1</sup>K. Gottfried and J. D. Jackson, *Nuovo Cimento* **33**, 309 (1964).

<sup>2</sup>J. T. Donohue and H. Högaasen, *Phys. Letters* **25B**, 554 (1967).

<sup>3</sup>J. D. Jackson, *Nuovo Cimento* **34**, 1646 (1964).

<sup>4</sup>M. Aderholz, J. V. Beaupre, M. Deutschmann, H. Grassler, R. Speth, H. Bottcher, C. Grote, K. Lanius, H. Schiller, A. Angelopoulos, K. W. J. Barnham, V. T. Cocconi, P. F. Dalpiaz, J. D. Hansen, G. Kellner, W. Kittel, D. R. O. Morrison, and H. J. Schreiber, *Nucl. Phys.* **B24**, 509 (1970).

<sup>5</sup>International  $K^+$  collaboration: Birmingham-Glasgow-Oxford Collaboration, Brussels-CERN $K^+$  Collaboration, University of California at Berkeley, University of California at Los Angeles, University of Chicago, University of Illinois, Johns Hopkins University, and University of Rochester.

<sup>6</sup>M. K. Banerjee and C. A. Levinson, *Ann. Phys. (N. Y.)* **2**, 499 (1957).

<sup>7</sup>D. R. Inglis, (a) *Phys. Letters* **10**, 336 (1964); (b) in

*Preludes in Theoretical Physics in Honor of V. F. Weisskopf*, edited by A. de-Shalit, L. Van Hove, and H. Feshbach (North-Holland, Amsterdam, 1966); (c) *Phys. Rev.* **142**, 591 (1966); (d) *ibid.* **157**, 873 (1967).

<sup>8</sup>See footnotes 1 and 2 in Ref. 7(c).

<sup>9</sup>P. Herquet and T. Trippe, CERN Report No. D. Ph. II/PHYS 70-29, 1970 (unpublished).

<sup>10</sup>R. Mercer, P. Antich, A. Callahan, C.-Y. Chien, B. Cox, R. Carson, D. Denegri, L. Ettliger, D. Feiok, G. Goodman, J. Haynes, A. Pevsner, R. Sekulin, V. Sreedhar, L. Resvanis, and R. Zdanis, *Bull. Am. Phys. Soc.* **15**, 658 (1970).

<sup>11</sup>S. B. Treiman and C. N. Yang, *Phys. Rev. Letters* **8**, 140 (1962).

<sup>12</sup>B. Barish, R. Gomez, J. Pine, S. Loken, T. Borak, R. Juhala, E. Malamud, D. Davies, P. Schlein, and W. Slater (unpublished).

<sup>13</sup>See, for example, summaries by L. D. Roper, R. M. Wright, and B. T. Feld, *Phys. Rev.* **138**, B190 (1965); P. Bareyre, C. Bricman, and G. Villet, *ibid.* **165**, 1730 (1968).